Bundle dynamics of interacting polar rods

Sumanth Swaminathan,[1,2] Dmitry Karpeev,[2] and Igor S. Aranson[3]
[1]*Engineering Sciences and Applied Mathematics, Northwestern University, 2145 Sheridan Road, Evanston, Illinois 60202, USA*
[2]*Mathematics and Computer Science Division, Argonne National Laboratory, Argonne, Illinois 60439, USA*
[3]*Materials Science Division, Argonne National Laboratory, Argonne, Illinois 60439, USA*
(Received 24 January 2008; published 9 June 2008)

We use a probabilistic model of microtubule interaction via molecular motors to study microtubule bundle interaction. Our model indicates that initially disordered systems of interacting polar rods exhibit an orientational instability resulting in spontaneous ordering. We study the existence and dynamic interaction of microtubule bundles analytically and numerically. Our results show a long term attraction and coalescing of bundles indicating a clear coarsening in the system; Microtubule bundles concentrate into fewer orientations on a slow logarithmic time scale.

DOI: 10.1103/PhysRevE.77.066206 PACS number(s): 05.65.+b, 87.16.−b

I. INTRODUCTION

Biological microtubules have been observed to form complex structures via interaction with molecular motors. Some examples include the formation of cellular cytoskeleton of daughter cells during cell division [1] and the assembly of mitotic spindles, which are used by eukaryotic cells to segregate chromosomes correctly during cell division [2]. In each of these instances, microtubules undergo motor mediated attachment, cross-linking, and sliding which ultimately leads to the formation of intricate structures [3]. Similar assemblies occur in filopodia formation in which actin filaments are cross-linked into bundles via interaction with active motor and static cross-linking proteins [4].

To understand the details of microtubule self-organization, researchers have performed a number of *in vitro* experiments [5–10] to study interactions of molecular motors and microtubules in isolation from other simultaneously occurring biophysical processes. These experiments have provided a qualitative picture of motor-filament interaction. After a molecular motor binds to a microtubule, it marches along the tubule length until it unbinds, causing minimal displacement of microtubules (motor run time after binding is approximately one second [2]). If, however, a molecular motor binds to two microtubules (most molecular motors have at least two binding sites), it can change their mutual position and orientation significantly [11]. Microtubule length, although constantly adjusting during the course of cell functioning through polymerization/depolymerization of tubulin dimers, can be as high as 40–60 microns with a diameter of the order of 20 nm. The thermal persistence length of a microtubule is of the order of a few millimeters (greatly exceeding the filament length) implying that microtubules are virtually unbendable by thermal fluctuations.

In small-scale simulations [8], interaction of rodlike filaments by means of motor binding has been studied, and patterns resembling experimental ones have been observed. In Ref. [12], a model including transport of molecular motors along microtubules and motor-induced microtubule alignment was proposed. Simulations showed that asters and vortices form in this model. More general models including variable bound and unbound motor density have been presented in Refs. [13,14].

In Ref. [15], Aranson and Tsimring studied a continuum model for the spatiotemporal dynamics of microtubules beginning with the derivation of a master equation for interacting polar rods. Microtubule interactions are treated as instantaneous inelastic rod collisions accompanied by spatial and angular drift associated with thermal fluctuations. The model exhibits an onset of orientational order for large-enough density of microtubules and molecular motors, formation of vortices, and then asters with an increase in the molecular motors concentration, in qualitative agreement with experiments.

In Refs. [16,17], Ben-Naim and Krapivsky derive in Fourier space an exact steady-state solution to the spatially homogeneous master equation presented in Ref. [15]. The authors further compute a critical diffusion coefficient marking a transition zone from ordered to disordered behavior as indicated by the order parameter, the mean orientation. Their result indicates that alignment becomes progressively stronger upon reduction of diffusion, ultimately yielding a bundle solution in rod density.

In this paper, we study the nonlinear dynamics of the spatially homogeneous master equation given that the range of angular interaction is small. This limit is interesting because simulations in the case of single motor-induced alignment have shown the onset of many localized bundles [18]. Understanding the dynamics of these various rod clusters yields insight into how bundles of similar orientation interact. The main result is that bundles have exponentially weak attraction accompanied by coalescing.

The paper is organized as follows. In Sec. II, we recall the spatially homogeneous rod alignment model proposed by Aranson and Tsimring, derive a limiting case for small angle interactions, and carry out linear stability analysis about the uniform state. An exact solution to the steady state problem is presented in Appendix A. In Sec. III we discuss the framework for the asymptotic analysis of bundle interaction. The results of the asymptotics are compared with numerical experiments. We conclude the study in Sec. IV with a discussion of results and open research questions.

II. ROD ALIGNMENT MODEL

In the model introduced by Aranson and Tsimring [15], rods of orientation θ are aligned through irreversible pair-

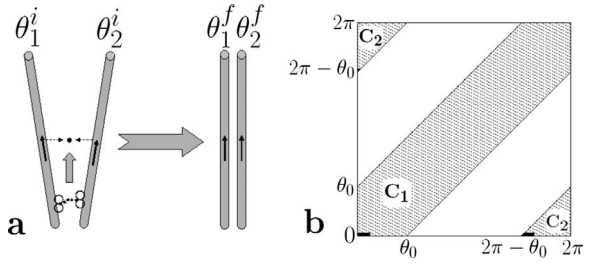

FIG. 1. (a) Depiction of motor mediated microtubule interaction and alignment for fully inelastic collisions. (b) Integration regions $C_{1,2}$ for Eq. (1).

wise interactions. These motor mediated inelastic interactions are treated as instantaneous collisions in which each rod changes its orientation according to the following collision rule:

$$\begin{pmatrix} \theta_1^f \\ \theta_2^f \end{pmatrix} = \begin{pmatrix} \gamma & 1-\gamma \\ 1-\gamma & \gamma \end{pmatrix} \begin{pmatrix} \theta_1^i \\ \theta_2^i \end{pmatrix},$$

where $\theta_{1,2}^i$ are the two rods' orientations before collision and $\theta_{1,2}^f$ are the orientations after. The constant γ characterizes the inelasticity of collisions (analog of the restitution coefficient in granular media). The angle between two rods is reduced after collision by an "inelasticity" factor $\epsilon = 2\gamma - 1$. Purely inelastic collisions correspond to $\gamma = \frac{1}{2}$ or $\epsilon = 0$. In this analysis, we assume that two rods interact only if the precollision angle between the rods is smaller than θ_0; this requirement, after taking into consideration 2π periodicity in alignment, gives the following interaction criteria: $|\theta_2^i - \theta_2^i| < \theta_0 < \pi$ and $2\pi - \theta_0 < |\theta_2^i - \theta_2^i| < 2\pi$. Hence, if a pair of rods intersects by the aforementioned collision rules, then the two interact inelastically, each rod acquiring the average orientation $\theta_1^f = \theta_2^f = \frac{\theta_1^i + \theta_2^i}{2}$. Rods are further allowed random wiggling characterized by rotational diffusion. Since the diffusion of small motors is about two orders of magnitude higher than that of large and heavy microtubules, spatial variations in motor density are neglected.

Consider $P(\theta, t)$ to be the probability distribution function of rods with orientation θ at time t, with normalizing condition $\int_{-\pi}^{\pi} P d\theta = 1$. Then, the master equation governing the spatially homogeneous self-organization of microtubules is given by

$$P_t = DP_{\theta\theta} + g \int_{C_1} P(\theta_1) P(\theta_2) \left[\delta\left(\theta - \frac{\theta_1}{2} - \frac{\theta_2}{2} \right) - \delta(\theta - \theta_2) \right] d\theta_1 d\theta_2 + g \int_{C_2} P(\theta_1) P(\theta_2) \times \left[\delta\left(\theta - \frac{\theta_1}{2} - \frac{\theta_2}{2} - \pi \right) - \delta(\theta - \theta_2) \right] d\theta_1 d\theta_2, \quad (1)$$

where D is the rotational diffusion coefficient describing thermal fluctuations of the rod orientation and g is the collision rate or the probability of two tubules interacting via molecular motors. The integration regions C_1 and C_2 are shown in Fig. 1 below. Integrating the δ functions and taking $\omega = \theta_2 - \theta_1$ yields

$$P_t = DP_{\theta\theta} + g \int_{-\theta_0}^{\theta_0} \left[P\left(\theta + \frac{\omega}{2} \right) P\left(\theta - \frac{\omega}{2} \right) - P(\theta) P(\theta - \omega) \right] d\omega. \quad (2)$$

The "collision" integral in Eq. (2) accounts for interaction with gains associated with rods aligning to obtain the orientation θ and losses due to rods having orientation θ before alignment.

In the case of collisions occurring only between rods initially having near alignment, one can consider θ_0 to be small. This limit is employed in order to study the onset of microtubule bundles of varying orientations. For small θ_0, the collision integral in Eq. (2) can be computed via Taylor expansion of P about $\omega = 0$ as follows:

$$P(\theta + \omega) = P(\theta) + \omega P' + \frac{\omega^2}{2} P'' + \frac{\omega^3}{6} P''' + \cdots. \quad (3)$$

The resulting form of the collision integral in Eq. (2) is

$$\int_{-\theta_0}^{\theta_0} \left[P\left(\theta - \frac{\omega}{2} \right) P\left(\theta + \frac{\omega}{2} \right) - P(\theta) P(\theta - \omega) \right] d\omega = \int_{-\theta_0}^{\theta_0} \left[-\omega P P' - \frac{\omega^2}{4} (P P'' + P''^2) + \omega^4 \left(\frac{-7}{192} P'''' P - \frac{1}{48} P' P''' + \frac{1}{64} P''^2 \right) \right] d\omega. \quad (4)$$

We keep up to fourth order terms in ω to offset the unstable backward nonlinear diffusion resulting from keeping only $O(\omega^2)$ terms. Computing the integral in Eq. (4) and rearranging the derivatives in θ yields a fourth-order nonlinear PDE which will be referred to henceforth as the small angle master equation

$$P_t(\theta) = D \frac{d^2 P}{d\theta^2} - g \frac{\theta_0^3}{12} \left\{ \frac{d^2}{d\theta^2} (P^2) + \frac{\theta_0^2}{80} \left[7 \frac{d^4}{d\theta^4} (P^2) - 24 \frac{d^2}{d\theta^2} \left(\frac{dP}{d\theta} \right)^2 \right] \right\}. \quad (5)$$

Clearly the uniform density of $P = P_0 = \frac{1}{2\pi}$ is a solution to Eq. (5) and represents the disordered state. For subcritical values $D < \bar{D}$ of the diffusion parameter, the uniform state losses its stability resulting in the onset of spontaneous orientation. Linear stability analysis reveals the unstable angular modes (as a function of the physical parameters). Taking $P = P_0 + \epsilon \tilde{P}$, and keeping $O(\epsilon)$ terms in Eq. (5) yields the linearized equation

$$\tilde{P}_t(\theta) = D \frac{d^2 \tilde{P}}{d\theta^2} - \frac{g P_0 \theta_0^3}{6} \frac{d^2 \tilde{P}}{d\theta^2} - \frac{7 g P_0 \theta_0^5}{480} \frac{d^4 \tilde{P}}{d\theta^4}. \quad (6)$$

Solutions to Eq. (6) of the form $\tilde{P} = e^{ik\theta + \lambda t}$, $k \neq 0$ exist for k and λ satisfying the dispersion relation

$$\lambda = k^2\left[-k^2\left(\frac{7gP_0\theta_0^5}{480}\right)+\left(\frac{gP_0\theta_0^3}{6}-D\right)\right].$$

Unstable modes are identified by the condition $\lambda > 0$ leading to the instability condition of the wave number k in terms of the physical parameters

$$|k| < \sqrt{\frac{80}{\theta_0^2}\left[1-\frac{6D}{7gP_0\theta_0^3}\right]}. \quad (7)$$

The parameters used in all numerical and analytical analyses to follow are $g=100$, $D=0.1$, $\theta_0=0.5$, $P_0=\frac{1}{2\pi}$. Substituting these parameters into Eq. (7) indicates that wave numbers of $k\approx 18$ and smaller yield instability in the linear limit.

The steady state small angle master equation can be solved both analytically as well as numerically. First, we rescale the independent and dependent variables to eliminate as many parameters as possible. Upon substitution of the scalings

$$\tilde{t} = t\left(\frac{10D}{3\theta_0^2}\right), \quad \tilde{\theta} = \theta\left(\sqrt{\frac{10}{3}}\frac{1}{\theta_0}\right), \quad \tilde{P} = P\left(\frac{\theta_0^3 g}{12D}\right), \quad (8)$$

we obtain the dimensionless small angle master equation (tildes are removed for brevity.),

$$P_t(\theta) = \frac{d^2P}{d\theta^2} - \frac{d^2}{d\theta^2}(P^2) - \frac{7}{24}\frac{d^4}{d\theta^4}(P^2) + \frac{d^2}{d\theta^2}\left[\left(\frac{dP}{d\theta}\right)^2\right]. \quad (9)$$

The exact steady state solution to Eq. (9) is derived in Appendix A. This solution, however, is of limited value to our analysis as it contains many constants of integration that are difficult to resolve analytically while the solution is in integral form. Instead, we rely on numerical treatment of Eq. (9) to gain insight into the structure of the steady state. Sample long time numerical states are shown in Fig. 2 below; these results are relevant in that they show the existence of localized bundles of well aligned rods. P, θ, and t axes in all of the figures are scaled subject to Eq. (8) [i.e., $0<\theta<2\pi$ becomes $0<\theta<2\pi(\sqrt{\frac{10}{3}}\frac{1}{\theta_0})$]

III. BUNDLE INTERACTION DYNAMICS

After the initial exponential growth of the instability, a well-defined multibundle configuration emerges in which the spatial scale is related to the characteristic length of the instability. The intermediate stage follows, characterized by movement and alignment of bundles which ultimately exhibit highly nonlinear interactions followed by coalescing of bundles. The final stages corresponding to bundles coalescing involve more complicated nonlinear behavior which is not considered in this publication.

In this study, we address the intermediate dynamics by preparing a two bundle initial state composed of two copies of a single bundle steady state configuration. This preparation is convenient because it allows us to skip the dynamics associated with shape change and focus on the movement. We expect, as indicated by our numerical studies, a quantifiable attracting interaction between bundles. This behavior

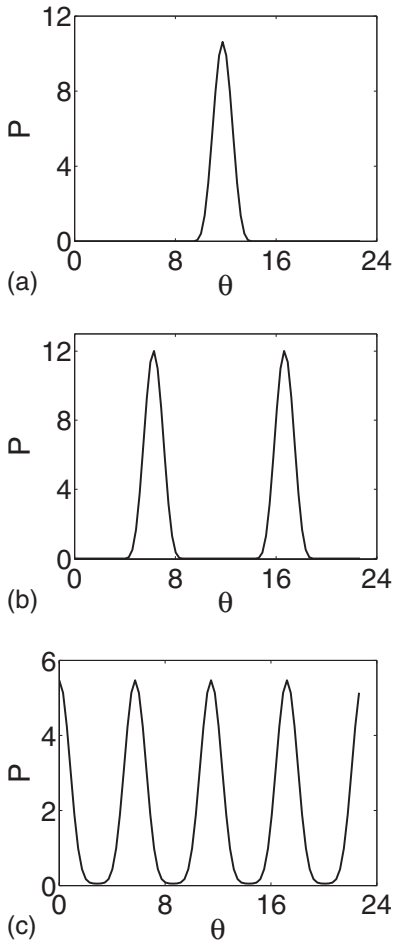

FIG. 2. Sample numerical long time bundle states computed from the small angle master equation. The initial conditions are small perturbations of the uniform state via unstable modes (as indicated by 7). The chosen parameters are $g=100$, $D=0.1$, $\theta_0=0.5$, $P_0=\frac{1}{2\pi}$.

is evident in our numerical simulations and is displayed in Fig. 3.

An analytical treatment of the early bundle dynamics is presented by considering two identical profiles initially centered far apart. In this large separation limit, the sum of two bundles can be considered an approximate steady state solution or leading order asymptotic steady state solution to Eq. (5). Hence, consider the following perturbation about a two bundle state:

$$P(\theta,t) = f_1(\theta) + f_2(\theta) - a + u(\theta,t), \quad f_i(\theta,t) = f_0[\theta - \theta_i(t)]. \quad (10)$$

Here, $f_0(\theta)$ is the profile of a single equilibrium bundle and a is the global minimum or the value approached by the tail. The function u is the unknown small correction. The value a is also small (verified numerically) and assumed to be of smaller order than f_i.

Substituting Eq. (10) into Eq. (5) yields

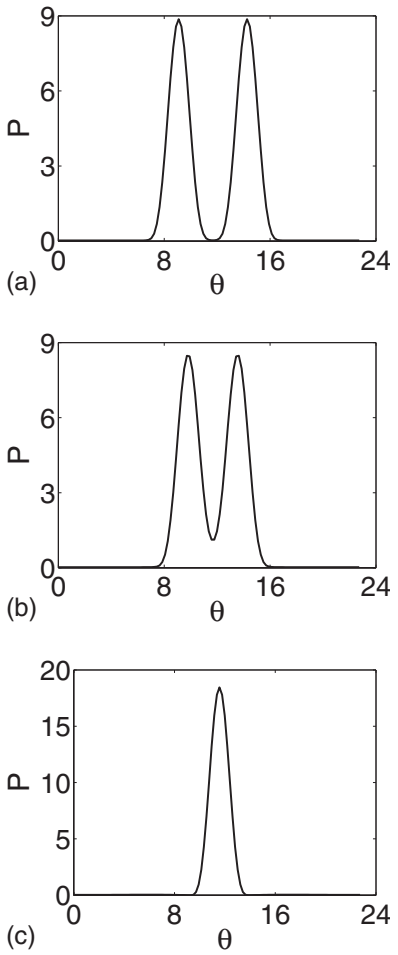

FIG. 3. Numerical data showing the time evolution and eventual coalescing of two bundles of well aligned rods of different orientation:(a) initial state, (b) coalescing bundles, (c) newly formed single bundle. The data indicates that the intermediate dynamics of bump interaction associated with movement is characterized by long term attraction.

$$-f_1'\frac{d\theta_1}{dt}-f_2'\frac{d\theta_2}{dt}+\frac{\partial u}{\partial t}=\frac{\partial^2 f_1}{\partial\theta^2}+\frac{\partial^2 f_2}{\partial\theta^2}+\frac{\partial^2 u}{\partial\theta^2}+[Q(f_1,f_1)+Q(f_2,f_2)+2Q(f_1+f_2,u)+2Q(f_1,f_2)-2Q(f_1+f_2,a)-2Q(a,u)]. \tag{11}$$

Here, we use the symmetric bilinear form

$$Q(X,Y)=\alpha\int_{-\tilde{\theta}_0}^{\tilde{\theta}_0}\left[X\left(\theta+\frac{\omega}{2}\right)Y\left(\theta-\frac{\omega}{2}\right)-\frac{1}{2}X(\theta)Y(\theta-\omega)-\frac{1}{2}X(\theta-\omega)Y(\theta)\right]d\omega,\quad(\alpha=1.97),\tag{12}$$

$$\left(\tilde{\theta}_0=\sqrt{\frac{10}{3}}\right)$$

to generate the quadratic collision integral $Q(P,P)$ in Eq. (2). The parameters α and $\tilde{\theta}_0$ come from inserting the scalings in Eq. (8) into Eq. (2).

Since f_1 and f_2 are solutions to the master equation, a number of terms can be eliminated leaving an equation for the correction u of the form

$$\frac{\partial^2 u}{\partial\theta^2}+2Q(f_1+f_2,u)=-\left(f_1'\frac{d\theta_1}{dt}+f_2'\frac{d\theta_2}{dt}+2Q(f_1,f_2)-2Q(f_1+f_2,a)\right).\tag{13}$$

Many assumptions are inherent in Eq. (13). First, the time evolution of the correction shape u_t and the collision term $Q(a,u)$, are both ignored because they are assumed to be of smaller order. Second, the mixed collision term, $Q(f_1,f_2)$ is kept because although f_1 and f_2 are O(1), their product is small due to the separation assumption. Third, the motion of the centers of each bundle given by the terms $\frac{d\theta_i}{dt}$ are assumed to be of the same order as the correction u.

Insight into the relative bundle motion is gained through an application of the Fredholm alternative. The existence of nontrivial solutions to Eq. (13) demands the orthogonality of the inhomogeneous terms on the right-hand side of Eq. (13) to the kernel of the homogeneous adjoint equation. In this case, as the homogeneous operator acting on u in Eq. (13) is self-adjoint, one can simply look for solutions of the equation

$$\frac{\partial^2 u}{\partial\theta^2}+2Q(f_1+f_2,u)=0.\tag{14}$$

Here, an approximate solution to Eq. (14) is the derivative of each individual bundle. Generally, because the master equation is translationally invariant, the derivative of a solution to the steady state master equation is a solution to the steady state linearized master equation.

Now, in Eq. (14), since (f_1+f_2) is not a solution, the aforementioned argument cannot be applied. However, consider the derivative of an individual bundle f_1. Substituting $u=\frac{\partial f_1}{\partial\theta}$ into Eq. (14) yields

$$\frac{\partial^2}{\partial\theta^2}\frac{\partial f_1}{\partial\theta}+2Q\left(f_1,\frac{\partial f_1}{\partial\theta}\right)+2Q\left(\frac{\partial f_1}{\partial\theta},f_2\right)=0.\tag{15}$$

If the third term on the left-hand side of Eq. (15) were absent, we would conclude that f_1' is a solution to Eq. (14). In fact, since the third term is of smaller order as it contains the product of f_1 and f_2, we can consider $u=\frac{\partial f_1}{\partial\theta}$ to be a leading order asymptotic solution to Eq. (14).

Now, applying the Fredholm alternative to Eq. (13) yields the following orthogonality condition:

$$\int_{-\tilde{\pi}}^{\tilde{\pi}}\frac{\partial f_i}{\partial\theta}\left(f_1'\frac{d\theta_1}{dt}+f_2'\frac{d\theta_2}{dt}+2Q(f_1,f_2)-2Q(f_1+f_2,a)\right)=0,\tag{16}$$

where the bounds of integration are taken from $-\tilde{\pi}$ to $\tilde{\pi}$, $\tilde{\pi}=(\theta_0\sqrt{\frac{10}{3}})\pi$, because of the θ-scaling in Eq. (8). Careful manipulation of Eq. (16) leads to an expression for the velocity at which f_1 and f_2 move toward one another. The details of this calculation are shown in Appendix B.

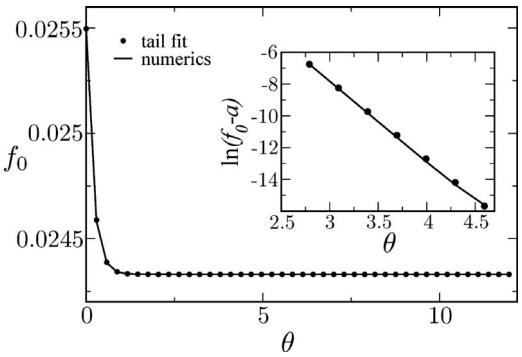

FIG. 4. Comparison of the numerical bundle tail to the fit. Here, the parameters computed are $a=0.0243$, $k=7.3$, $b=1.6\times10^6$. The value of k when computed from the linear approximation is $k=7.9$. This is in qualitative agreement with the optimal fit value of $k=7.3$.

A. Introduction of exponential tail

The velocities of the centers of each bundle are given by $\frac{d\theta_i}{dt}$. As both θ_1 and θ_2 are embedded in the collision integral terms of Eq. (16), we must find a way to extract them to yield a manageable differential equation. This is done by utilizing the fact that the shape of each bundle profile far from the center can be approximated by an exponentially decaying tail. Suppose the following form for the tail:

$$f_0(\theta) = a + be^{-k|\theta|}, \quad |\theta| > q, \tag{17}$$

where q is the distance from the center of the bundle at which the exponential tail approximation is legitimate. A plot of the fit of the numerically determined bundle solution to the anzats given in Eq. (17) is shown in Fig. 4.

Now, we must changed variables of integration in Eq. (16) term by term to utilize Eq. (17) and solve for the relative bundle velocity. An exhaustive derivation of the relative velocity is shown in Appendix B. Proceeding in the fashion outlined in the appendix yields a simple ordinary differential equation for the relative bundle distance $X=\theta_2-\theta_1$ of the form

$$\frac{dX}{dt} = c_1 e^{-kX} \tag{18}$$

where the integral expression for c_1 is shown in Appendix B. Equation (18) indicates a growth in relative velocity as the bundles become more nearly aligned. We solve for X through a simple separation of variables to obtain

$$X = \frac{1}{k}\ln|c_1 kt + e^{kX_0}|. \tag{19}$$

Figure 5(a) below shows the time evolution of the relative distance between two bundles as they move toward each other; Fig. 5(b) shows the calculated value of c_1 for various $\tilde{\theta}_0$, and Fig. 5(c) shows the time evolution of an initial set of many bundles. The growth of c_1 with larger $\tilde{\theta}_0$ in Fig. 5(b) is consistent with the notion that larger $\tilde{\theta}_0$ yields greater interaction.

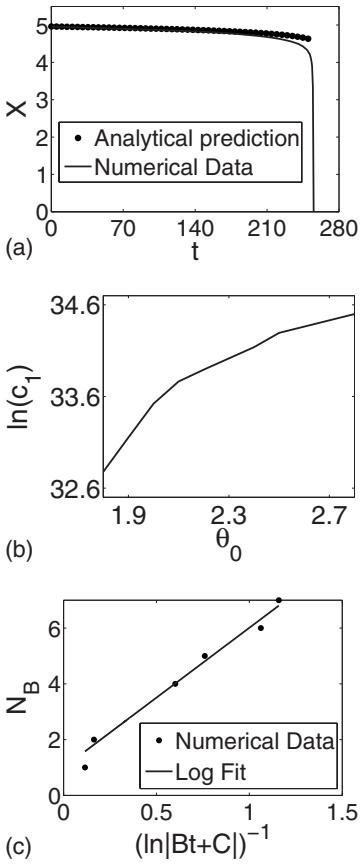

FIG. 5. (a) Comparison between the numerical and analytical predictions of the time evolution of the relative distance between bundles, (b) c_1 as a function of θ_0. c_1 represents the decay rate in the relative distance X, the growth of c_1 with increasing θ_0 indicates that bundles coalesce more easily when greater interaction angles are accepted, (c) time evolution of the number of bundle orientations; the fit parameters are $A=5.01$, $B=1.94$, $C=-1.50$.

The data in Fig. 5(c) is fit to a function of the form $(1+\frac{A}{\ln|Bt+C|})$, with fitting parameters A,B,C. This form was chosen because we know that the number of bundles scales as $N\sim\frac{L}{X}$, where L is the domain length and X is the distance between bundles; the distance between bundles changes logarithmically with time as indicated by Eq. (19).

The coalescing of bundles observed in simulations of two bundle and multibundle configurations indicates that coarsening in the system occurs on a slow logarithmic time scale. This finding is well illustrated in Figs. 5(a) and 5(c). Similar techniques for studying coarsening have been used in the study of axial segregation of granular materials. In Ref. [19], the authors show that bands of granular material coarsen on a similar logarithmic scale. Likewise, in Ref. [20], the authors find slow coarsening when studying the dynamics of slurries in circular and square tubes. When studied in complex, higher-dimensional geometries, bands of segregated material have been known to exhibit slow coarsening but with more complicated dynamics [21]. Long term bundle formation is known to occur in liquid crystal systems as well; however, ordering in such systems is due mostly to thermodynamic considerations as opposed to active motor mediated effects [22].

IV. CONCLUSIONS

In this paper, we modified the rod alignment model proposed in Ref. [15] to yield a master equation governing the self-organization of microtubules for near alignment interactions. We found that initially disordered systems exhibit an ordering instability resulting in the onset of bundles of similarly oriented microtubules. The phenomenon of multiple oriented states called bundles in this publication were not studied in previous models allowing for collisions between microtubules having a larger range of interaction angles.

The primary result of this study is the derivation of an expression governing the relative motion of bundles. Both the numerical simulations as well as the asymptotic methods show that bundles initially situated far from one another exhibit attractive behavior. The subsequent coalescing shows a coarsening in the system as bundles become concentrated in fewer orientations. The time scale of coarsening in two bundle and multibundle configurations is shown to be logarithmic.

The asymptotic calculations governing the time evolution of the relative distance between bundles shows good quantitative agreement with numerical simulations. Deviations in the analytical work from the numerics occur only when bundles are nearly aligned. This is, of course, expected as the asymptotics are accurate only when applied to bundles at large relative distances. Further numerical simulations showed that the speed at which bundles move toward each other increases with increasing θ_0. This finding is in qualitative agreement with simulations allowing for interactions between all precollision orientations.

Many additional questions are yet to be addressed. First, we derived an exact integral solution to the small angle master equation. We are yet to obtain a great deal of meaning from it, and further analysis could be useful, particularly in understanding the type, number, and long time behavior of the numerically determined bundle states. Furthermore, we considered no spatial variations in either motor or microtubule density in this paper nor did we relax the assumption of exclusively binary microtubule interactions. With the inclusion of spatial inhomogeneity, one could explore the critical parameter space at which rods become disordered and derive in a similar fashion to that of Aranson and Tsimring [15] a couple system of Ginzburg-Landau equations in the limit of small angle interactions. Finally, the methods used to obtain quantitative information about the dynamics of bundle motion do not incorporate noise associated with diffusive effects. In addition to the translation and eventual coalescing of bundles, there also exists small scale fluctuations in the bundles' positions and shapes associated with thermal effects. These effects could be more carefully incorporated into the dynamics model.

Ultimately, although our analysis is problem specific, we believe that the concept of inelastic collisions in angle space resulting in alignment of rod directions is a primary mechanism driving self-organization in many physical systems. A few examples include rod-shaped swimming bacteria or vibrated granular rod systems. Further investigation and modifications of our models could provide deeper insight into other physical processes.

ACKNOWLEDGMENTS

The authors would like to thank Alexander Golovin and Eli Ben-Naim for useful discussions throughout the period of this study. This work was supported by the U.S. Department of Energy, Grants No. DE-AC02-06CH11357.

APPENDIX A: SMALL ANGLE MASTER EQUATION ANALYTICAL SOLUTION

A steady state analytical solution to Eq. (5) can be found by assuming the following ansatz:

$$P(\theta) = h(\theta)^{\alpha}, \quad \alpha = \text{const.} \tag{A1}$$

Substituting this expression into Eq. (9) (after integrating twice) we obtain

$$\tilde{C} = h^{\alpha} - h^{2\alpha} - \frac{7}{24}[2\alpha(2\alpha-1)h^{2\alpha-2}h'^2 + 2\alpha h^{2\alpha-1}h''] + \alpha^2 h^{2\alpha-2}h'^2. \tag{A2}$$

Here, one of the integration constants is killed so as to eliminate the linear term in θ and preserve 2π periodic solutions. Now, Eq. (A2) can be solved analytically if the first derivative terms are absent. This is achieved by choosing α as is done below:

$$\alpha^2 - \frac{7}{24}(4\alpha^2 - 2\alpha) = 0, \quad \alpha = \frac{7}{2}. \tag{A3}$$

Substituting for α and solving the resulting ODE yields

$$\tilde{C} = h^{7/2} - h^7 - \frac{49}{24}h^6 h'' \int \frac{dh}{\sqrt{-\frac{h^2}{2} - \frac{2}{3}h^{-3/2} - \frac{\tilde{C}}{5}h^{-5} + \tilde{C}_1}} = \frac{48}{49}\theta + \tilde{C}_2. \tag{A4}$$

APPENDIX B: RELATIVE BUNDLE VELOCITY CALCULATION

In order to analyze the orthogonality condition given in Eq. (16), we must expand the collision integral terms as follows:

$$\frac{d\theta_1}{dt}\int_{-\tilde{\pi}}^{\tilde{\pi}}\left(\frac{\partial f_1}{\partial\theta}\right)^2 d\theta + \frac{d\theta_2}{dt}\int_{-\tilde{\pi}}^{\tilde{\pi}}\frac{\partial f_1}{\partial\theta}\frac{\partial f_2}{\partial\theta}d\theta = \int_{-\tilde{\pi}}^{\tilde{\pi}}\frac{\partial f_1}{\partial\theta}[-2Q(f_1,f_2)+2Q(f_1+f_2,a)]d\theta$$

$$= -\frac{\alpha}{2}\int_{-\tilde{\pi}}^{\tilde{\pi}}\int_{-\tilde{\theta}_0}^{\tilde{\theta}_0} f_0'(\theta-\theta_1)\left[2f_0\left(\theta-\theta_1+\frac{\omega}{2}\right)f_0\left(\theta-\theta_2-\frac{\omega}{2}\right)-f_0(\theta-\theta_1)f_0(\theta-\theta_2-\omega)\right.$$

$$\left.-f_0(\theta-\theta_1-\omega)f_0(\theta-\theta_2)\right]d\omega d\theta + \frac{\alpha}{2}\int_{-\tilde{\pi}}^{\tilde{\pi}}\int_{-\tilde{\theta}_0}^{\tilde{\theta}_0} f_0'(\theta-\theta_1)\left[2af_0\left(\theta-\theta_1+\frac{\omega}{2}\right)-af_0(\theta\right.$$

$$\left.-\theta_1)-af_0(\theta-\theta_1-\omega)\right]d\omega d\theta + \frac{\alpha}{2}\int_{-\tilde{\pi}}^{\tilde{\pi}}\int_{-\tilde{\theta}_0}^{\tilde{\theta}_0} f_0'(\theta-\theta_1)\left[2af_0\left(\theta-\theta_2+\frac{\omega}{2}\right)-af_0(\theta\right.$$

$$\left.-\theta_2)-af_0(\theta-\theta_2-\omega)\right]d\omega d\theta. \tag{B1}$$

The third integral is of smaller order than the other terms because the products include a, f_1, and f_2. Similarly, the second term on the left hand side of Eq. (B1) is of smaller order because the product includes f_1, f_2, and $\frac{d\theta_2}{dt}$.

Consider the first term on the right hand side of Eq. (B1). Let, $\tilde{\theta}=\theta-\theta_1$. Then,

$$2\int_{-\tilde{\pi}}^{\tilde{\pi}}\int_{-\tilde{\theta}_0}^{\tilde{\theta}_0} f_0'(\theta-\theta_1)f_0\left(\theta-\theta_1+\frac{\omega}{2}\right)f_0\left(\theta-\theta_2-\frac{\omega}{2}\right)d\omega d\theta$$

$$= 2\int_{-\tilde{\pi}}^{\tilde{\pi}}\int_{-\tilde{\theta}_0}^{\tilde{\theta}_0} f_0'(\tilde{\theta})f_0\left(\tilde{\theta}+\frac{\omega}{2}\right)(a+be^{-k|\tilde{\theta}-\omega/2-(\theta_2-\theta_1)|})d\omega d\tilde{\theta}, \tag{B2}$$

assuming that $|\tilde{\theta}-\frac{\omega}{2}-(\theta_2-\theta_1)|>q$. This assumption holds true for most of the domain because $(\theta_2-\theta_1)$ is large. Note also that the integration bounds do not change when integrating over $\tilde{\theta}$ because the integrand is $2\tilde{\pi}$ periodic. Now, what happens when $|\tilde{\theta}-\frac{\omega}{2}-(\theta_2-\theta_1)|<q$? Integrating over this region of consideration, and taking, $\bar{\theta}=\tilde{\theta}-(\theta_2-\theta_1)$, yields

$$2\int_{-q+\omega/2+(\theta_2-\theta_1)}^{q+\omega/2+(\theta_2-\theta_1)}\int_{-\tilde{\theta}_0}^{\tilde{\theta}_0} f_0'(\tilde{\theta})f_0\left(\tilde{\theta}+\frac{\omega}{2}\right)f_0$$

$$\times\left(\tilde{\theta}-\frac{\omega}{2}-(\theta_2-\theta_1)\right)d\omega d\tilde{\theta}$$

$$= 2\int_{-q+\omega/2}^{q+\omega/2}\int_{-\tilde{\theta}_0}^{\tilde{\theta}_0}\left[\frac{\partial}{\partial\bar{\theta}}(a+be^{-k|\bar{\theta}+(\theta_2-\theta_1)|})\right]$$

$$\times(a+be^{-k|\bar{\theta}+\omega/2+(\theta_2-\theta_1)|})f_0\left(\bar{\theta}-\frac{\omega}{2}\right)d\omega d\bar{\theta}, \tag{B3}$$

assuming that $|\bar{\theta}+(\theta_2-\theta_1)|>q$ and $|\bar{\theta}+\frac{\omega}{2}+(\theta_2-\theta_1)|>q$. This is, of course, true on the whole region of integration because $(\theta_2-\theta_1)$ is much larger than both q and ω. Since both of the aforementioned terms are positive on the region of integration, the result in Eq. (B3) can be simplified further to yield

$$2\int_{-q+\omega/2}^{q+\omega/2}\int_{-\tilde{\theta}_0}^{\tilde{\theta}_0}(-kbe^{-k(\bar{\theta}+(\theta_2-\theta_1))})(a+be^{-k(\bar{\theta}+\omega/2+(\theta_2-\theta_1))})f_0$$

$$\times\left(\bar{\theta}-\frac{\omega}{2}\right)d\omega d\bar{\theta}. \tag{B4}$$

As both a and $e^{-k\bar{\theta}}$ are small terms, the integral over the smaller region represented in Eq. (B4) is of smaller order than that of the larger region represented in Eq. (B2) and can henceforth be ignored.

Similar adjustments to integration variables can be done on each of the terms left in Eq. (B1) to yield the following equation governing the velocity of f_1:

$$\frac{d\theta_1}{dt} = -\frac{\alpha}{\int_{-\tilde{\pi}}^{\tilde{\pi}}(f_0')^2 d\theta}\left[\int_{-\tilde{\pi}}^{\tilde{\pi}}\int_{-\tilde{\theta}_0}^{\tilde{\theta}_0} 2bf_0'(\theta)f_0\left(\theta+\frac{\omega}{2}\right)\right.$$

$$\times(e^{-k|\theta-\omega/2-(\theta_2-\theta_1)|})d\omega d\theta - \int_{-\tilde{\pi}}^{\tilde{\pi}}\int_{-\tilde{\theta}_0}^{\tilde{\theta}_0} bf_0'(\theta)f_0(\theta)$$

$$\times(e^{-k|\theta-\omega-(\theta_2-\theta_1)|})d\omega d\theta - \int_{-\tilde{\pi}}^{\tilde{\pi}}\int_{-\tilde{\theta}_0}^{\tilde{\theta}_0} bf_0'(\theta)f_0(\theta-\omega)$$

$$\left.\times(e^{-k|\theta-(\theta_2-\theta_1)|})d\omega d\theta\right]. \tag{B5}$$

A comparable expression governing the motion of f_2 can be derived in a similar fashion. In fact, one can show that the velocity of f_2 is the negative of that of f_1. First, consider the analog to Eq. (B1) for f_2:

$$\frac{d\theta_2}{dt}\int_{-\tilde{\pi}}^{\tilde{\pi}}\left(\frac{\partial f_2}{\partial\theta}\right)^2 d\theta = \int_{-\tilde{\pi}}^{\tilde{\pi}}\frac{\partial f_2}{\partial\theta}[-2Q(f_1,f_2)+2Q(f_1+f_2,a)]d\theta$$
$$= -\frac{\alpha}{2}\Bigg\{\int_{-\tilde{\pi}}^{\tilde{\pi}}\int_{-\tilde{\theta}_0}^{\tilde{\theta}_0} f_0'(\theta-\theta_2)\Bigg[2f_0\left(\theta-\theta_1+\frac{\omega}{2}\right)f_0\left(\theta-\theta_2-\frac{\omega}{2}\right)-f_0(\theta-\theta_1)f_0(\theta-\theta_2-\omega)-f_0(\theta-\theta_1-\omega)f_0(\theta-\theta_2)\Bigg]d\omega d\theta+\int_{-\tilde{\pi}}^{\tilde{\pi}}\int_{-\tilde{\theta}_0}^{\tilde{\theta}_0} f_0'(\theta-\theta_2)\times\Bigg[2af_0\left(\theta-\theta_1+\frac{\omega}{2}\right)-af_0(\theta-\theta_1)-af_0(\theta-\theta_1-\omega)\Bigg]\Bigg\}d\omega d\theta. \tag{B6}$$

Now, once again we do several changes of variables and utilize the exponential tail approximation to obtain the differential equation governing the motion of f_2.

$$\frac{d\theta_2}{dt} = \frac{\alpha}{\int_{-\tilde{\pi}}^{\tilde{\pi}}(f_0')^2 d\theta}\Bigg[\int_{-\tilde{\pi}}^{\tilde{\pi}}\int_{-\tilde{\theta}_0}^{\tilde{\theta}_0} 2bf_0'(\theta)f_0\left(\theta+\frac{\omega}{2}\right)\times(e^{-k|\theta-\omega/2-(\theta_2-\theta_1)|})d\omega d\theta-\int_{-\tilde{\pi}}^{\tilde{\pi}}\int_{-\tilde{\theta}_0}^{\tilde{\theta}_0} bf_0'(\theta)f_0(\theta)\times(e^{-k|\theta-\omega-(\theta_2-\theta_1)|})d\omega d\theta-\int_{-\tilde{\pi}}^{\tilde{\pi}}\int_{-\tilde{\theta}_0}^{\tilde{\theta}_0} bf_0'(\theta)f_0(\theta-\omega)\times(e^{-k|\theta-(\theta_2-\theta_1)|})d\omega d\theta\Bigg]. \tag{B7}$$

The relative distance, $X=\theta_2-\theta_1$, can be found by subtracting Eq. (B5) from Eq. (B7):

$$\frac{dX}{dt} = \frac{2\alpha}{\int_{-\tilde{\pi}}^{\tilde{\pi}}(f_0')^2 d\theta}\Bigg[\int_{-\tilde{\pi}}^{\tilde{\pi}}\int_{\tilde{\theta}_0}^{\tilde{\theta}_0} 2bf_0'(\theta)f_0\left(\theta+\frac{\omega}{2}\right)\times(e^{-k|\theta-\omega/2-X|})d\omega d\theta-\int_{-\tilde{\pi}}^{\tilde{\pi}}\int_{-\tilde{\theta}_0}^{\tilde{\theta}_0} bf_0'(\theta)f_0(\theta)\times(e^{-k|\theta-\omega-X|})d\omega d\theta-\int_{-\tilde{\pi}}^{\tilde{\pi}}\int_{\tilde{\theta}_0}^{\tilde{\theta}_0} bf_0'(\theta)f_0(\theta-\omega)\times(e^{-k|\theta-X|})d\omega d\theta\Bigg]. \tag{B8}$$

In order to solve Eq. (B8), each integration term on the right hand side must be divided into appropriate regions to eliminate the absolute value terms. Since this analysis only applies to large bundle separation distances, we replace the X inside the collision integrals with X_0 where X_0 is the initial separation distance. Numerical simulations have shown that this assumption is reasonable because the contribution to the integral associated with the region $\theta>X$ is many orders of magnitude smaller than that of the region $\theta<X$. Proceeding in this fashion yields a simple ordinary differential equation for X of the form

$$\frac{dX}{dt} = c_1 e^{-kX} + c_2 e^{kX}, \tag{B9}$$

where

$$c_1 = \frac{2\alpha}{\int_{-\tilde{\pi}}^{\tilde{\pi}}(f_0')^2 d\theta}\Bigg\{\Bigg[\int_{-\tilde{\pi}}^{\tilde{\pi}}\int_{-\tilde{\theta}_0}^{\tilde{\theta}_0} 2bf_0'(\theta)f_0\left(\theta+\frac{\omega}{2}\right)\times(e^{k(\theta-\omega/2)})d\omega d\theta\Bigg]_{(\theta-\omega/2<X_0)}-\Bigg[\int_{-\tilde{\pi}}^{\tilde{\pi}}\int_{-\tilde{\theta}_0}^{\tilde{\theta}_0} bf_0'(\theta)f_0(\theta)\times(e^{k(\theta-\omega)})d\omega d\theta\Bigg]_{(\theta-\omega<X_0)}-\Bigg[\int_{-\tilde{\pi}}^{\tilde{\pi}}\int_{-\tilde{\theta}_0}^{\tilde{\theta}_0} bf_0'(\theta)f_0(\theta-\omega)\times(e^{k\theta})d\omega d\theta\Bigg]_{(\theta<X_0)}\Bigg\} \tag{B10}$$

and

$$c_2 = \frac{2\alpha}{\int_{-\tilde{\pi}}^{\tilde{\pi}}(f_0')^2 d\theta}\Bigg\{\Bigg[\int_{-\tilde{\pi}}^{\tilde{\pi}}\int_{-\tilde{\theta}_0}^{\tilde{\theta}_0} 2bf_0'(\theta)f_0\left(\theta+\frac{\omega}{2}\right)\times(e^{-k(\theta-\omega/2)})d\omega d\theta\Bigg]_{(\theta-\omega/2>X_0)}-\Bigg[\int_{-\tilde{\pi}}^{\tilde{\pi}}\int_{-\tilde{\theta}_0}^{\tilde{\theta}_0} bf_0'(\theta)f_0(\theta)\times(e^{-k(\theta-\omega)})d\omega d\theta\Bigg]_{(\theta-\omega>X_0)}-\Bigg[\int_{-\tilde{\pi}}^{\tilde{\pi}}\int_{-\tilde{\theta}_0}^{\tilde{\theta}_0} bf_0'(\theta)f_0(\theta-\omega)\times(e^{-k\theta})d\omega d\theta\Bigg]_{(\theta>X_0)}\Bigg\}. \tag{B11}$$

Numerical integration of c_1 and c_2 shows that c_2 is many orders of magnitude smaller than c_1. Hence, the growing exponential term is ignored as it contributes (verified numerically) in no appreciable way to the solution of Eq. (18).

[1] J. Howard, *Mechanics of Motor Proteins and the Cytosceleton* (Springer, New York, 2000).
[2] L. C. Kapitein, E. J. G. Peterman, B. H. Kwok, J. H. Kim, T. M. Kapoor, and C. F. Schmidt, Nature (London) **435**, 114 (2005).
[3] D. Smith, F. Ziebert, D. Humphrey, C. Duggan, M. Steinbeck, W. Zimmermann, and J. Kas, Biophys. J. **93**, 4445 (2007).
[4] D. Vignjevic, D. Yarar, M. D. Welch, J. Peloquin, T. Svitkina, and G. G. Borisy, J. Cell Biol. **160**, 951 (2003).
[5] K. Takiguchi, J. Biochem. **109**, 250 (1991).
[6] R. Urrutia, M. A. McNiven, J. P. Albanesi, D. B. Murphy, and B. Kachar, Proc. Natl. Acad. Sci. U.S.A. **88**, 6701 (1991).
[7] F. J. Nédélec, T. Surrey, A. C. Maggs, and S. Leibler, Nature (London) **389**, 305 (1997).
[8] T. Surrey, F. Nédélec, S. Leibler, and E. Karsenti, Science **292**, 1167 (2001).
[9] D. Humphrey, C. Duggan, D. Saha, D. Smith, and J. Käs, Nature (London) **416**, 413 (2002).
[10] F. Nédélec, T. Surrey, and A. C. Maggs, Phys. Rev. Lett. **86**, 3192 (2001).
[11] In experiments [7,8] artificial molecular constructs that couple 4–8 motors using streptavidin-biotin links were used instead of isolated motors. However, it does not qualitatively change the mechanism of microtubule-motor interaction.
[12] H. Y. Lee and M. Kardar, Phys. Rev. E **64**, 056113 (2001).
[13] J. Kim, Y. Park, B. Kahng, and H. Y. Lee, J. Korean Phys. Soc. **42**, 162 (2003).
[14] S. Sankararaman, G. I. Menon, and P. B. Sunil Kumar, Phys. Rev. E **70**, 031905 (2004).
[15] I.S. Aranson and L.S. Tsimring, Phys. Rev. E **71**, 050901(R) (2005).
[16] E. Ben-Naim and P. L. Krapivsky, Phys. Rev. E **61**, R5 (2000).
[17] E. Ben-Naim and P. L. Krapivsky, Phys. Rev. E **73**, 031109 (2006).
[18] F. Ziebert, M. Vershinin, S. P. Gross, and I. Aranson (unpublished).
[19] I. S. Aranson, L. S. Tsimring, and V. M. Vinokur, Phys. Rev. E **60**, 1975 (1999).
[20] S. J. Fiedor and J. M. Ottino, Phys. Rev. Lett. **91**, 244301 (2003).
[21] T. Finger, A. Voigt, J. Stadler, H. G. Niessen, L. Naji, and R. Stannarius, Phys. Rev. E **74**, 031312 (2006).
[22] P. G. de Gennes and J. Prost, *The Physics of Liquid Crystals* (Clarendon Press, Oxford, 1993).